

Maghemite-Copper Nanocomposites: Applications for Ligand-Free Cross-Coupling (C–O, C–S, and C–N) Reactions

Rakesh K. Sharma,^{*[a]} Rashmi Gaur,^[a] Manavi Yadav,^[a] Anuj K. Rathi,^[b] Jiri Pechousek,^[b] Martin Petr,^[b] Radek Zboril,^[b] and Manoj B. Gawande^{*[b]}

A magnetically retrievable, efficient, and benign maghemite-Cu nanocatalyst was synthesized from inexpensive precursors and applied for C–O, C–N, and C–S bond-formation reactions. The obtained maghemite-Cu nanocatalyst was characterized by various techniques such as XRD, X-ray photoelectron spectroscopy, field-emission gun SEM with energy-dispersive spectroscopy,

atomic absorption spectroscopy, TEM, high-angle annular dark-field scanning transmission electron microscopy, FTIR spectroscopy, and Mössbauer spectroscopy. Excellent catalytic activity, ease of recovery, and reusability without a significant loss of yield make the present protocol highly sustainable to deal with industrial and environmental concerns.

Introduction

Since the era of the Wohler synthesis of urea, the demand for effective, competent, and sustainable practices to perform various organic transformations has been a major challenge in the world of chemical research.^[1] However, during the past few years, the integration of sustainable chemistry with precise nanotechnology has contributed significantly to the resolution of this problem by the introduction of supported heterogeneous nanocatalysts.^[2] This is because of the advantages provided by heterogeneous nanocatalysts, which include a high surface area, high metal loading, excellent stability, and the facile separation and recyclability of the catalyst.^[3] Thus, nowadays these supported nanocomposites are an integral major feature of catalysis science and technology, and most organic industrial chemistry relies on them.^[4] Consequently, there is a critical need for a superior and advanced heterogeneous nanocatalytic systems to perform various organic transformations. In this context, supported nanomaterials have been employed in several types of solid nanosupports, which include silica, alumina, iron oxide, polymers, and carbon.^[5,6] Of these, "iron oxides" have garnered much attention because of their unique characteristics, which include their nontoxic nature, chemical stability,

and economical viability as they can be prepared easily from low-cost precursors.^[7]

The most significant and unique characteristic is that they are magnetically separable, which offers a good alternative to filtration and centrifugation methods. These outstanding features impart radical and remarkable transformations in organic synthesis and drive researchers towards the design and development of new heterogeneous nanocatalysts.^[8–13] Recently, considerable attempts have been made towards selective C–heteroatom (C–O, C–N, and C–S) bond formation.^[14] These reactions are powerful tools for the formation of a variety of substrates that are of biological, pharmaceutical, industrial, and material interests.^[15] The cross-coupling reactions of different nucleophiles with aryl halides have been achieved by the Ullmann,^[16] Buchwald,^[17] Hartwig,^[18] Evans,^[19] and Chan methods.^[20] Among these, the classical Ullmann condensation reaction is efficient as it involves Cu as a catalyst, which often provides a high catalytic activity similar to expensive and toxic noble metals, such as Pd.^[21] Furthermore, the Ullmann reaction employs easily available aryl halide as the aryl donor in comparison to boronic acid and organotrifluoroborates, which are used in other reactions.^[19–22] However, their practical utility is hindered because of the involvement of harsh reaction conditions such as high temperatures, the use of expensive and complex ligands, the employment of single-use catalysts, and the low yields. Additionally, most of these catalyst are homogeneous and, therefore, not only cause the problem of catalyst separation and recycling but also lead to large amounts of waste on scale up.^[23]

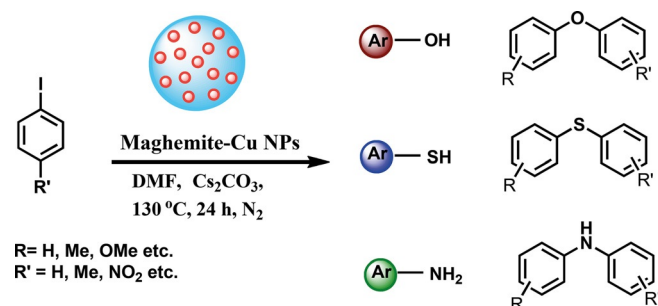
In the early 20th century, the discovery of heterogeneous catalysts, which include Pd,^[24] Cu,^[25] and Ni^[26] were reported as effective and reusable catalysts under much milder reaction conditions. Unfortunately, these existing heterogeneous catalysts proceed with the use of expensive ligands and tedious isolation procedures, such as centrifugation or filtration, for the re-

[a] Prof. R. K. Sharma, R. Gaur, M. Yadav
Green Chemistry Network Center
Department of Chemistry
University of Delhi
Delhi, 110007 (India)
E-mail: rksharmagreenchem@hotmail.com

[b] Dr. A. K. Rathi, Dr. J. Pechousek, M. Petr, Prof. R. Zboril, Dr. M. B. Gawande
Regional Centre of Advanced Technologies and Materials
Faculty of Science
Department of Physical Chemistry
Palacky University
Šlechtitelů 11, 783 71, Olomouc (Czech Republic)
E-mail: manoj.gawande@upol.cz

Supporting information for this article is available on the WWW under <http://dx.doi.org/10.1002/cctc.201500546>.

covery of the expensive metal catalyst. Consequently, one of the major challenges in chemical synthesis is to establish a promising method for C–heteroatom bond formation that circumvents these problems. Thus, in pursuit of our research interests in the design and synthesis of nanocatalysts based on iron oxides for various benign organic transformations,^[27,28] herein we describe the fabrication, characterization, and applications of a maghemite-supported Cu nanocatalyst for three different types of coupling reactions, O–aryl, N–aryl, and S–aryl (Scheme 1).



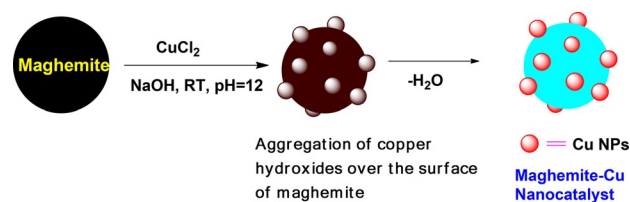
Scheme 1. Maghemite-Cu-catalyzed cross-coupling (C–O, C–S, and C–N) reactions.

Notably, this catalytic system is a simple yet effective approach as it avoids several multistep postsynthetic functionalization processes and the use of toxic and complex ligands, which thus renders the present protocol straightforward, superior, and cost effective.

Results and Discussion

Characterization techniques

The maghemite-Cu nanocatalyst was prepared by a simple wet impregnation technique followed by dehydration^[29] (Scheme 2) and characterized by XRD, atomic absorption spec-



Scheme 2. Synthesis of the maghemite-Cu nanocatalyst.

trosopy (AAS), TEM, field-emission gun scanning electron microscopy with energy-dispersive spectroscopy (FEG-SEM-EDS), X-ray photoelectron spectroscopy (XPS), Mössbauer spectroscopy, and high-angle annular dark-field scanning transmission electron microscopy (HAADF-STEM).

The powder XRD profiles of maghemite and maghemite-Cu are depicted in Figure 1; the crystallite size of the catalyst was determined by the Debye–Scherrer equation to be 28.7 nm,

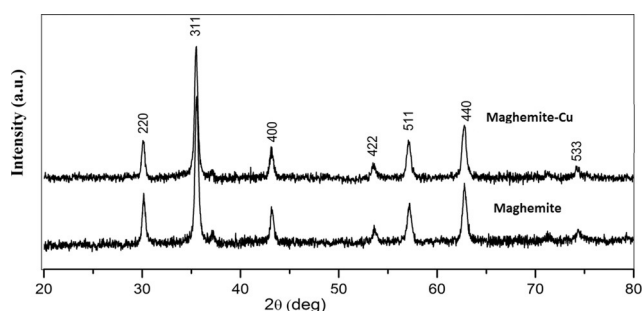


Figure 1. XRD patterns of maghemite and the maghemite-Cu nanocatalyst.

which is in agreement with the result obtained from TEM (20–40 nm). The peaks observed in the XRD pattern at $2\theta = 220$, 311, 400, 422, 511, and 440 are attributed to maghemite. Although magnetite (Fe_3O_4) and maghemite ($\gamma\text{-Fe}_2\text{O}_3$) have the same spinel arrangement and their XRD peak locations are quite close to each other, further characterization by Mössbauer spectroscopy, which clearly showed that the sample does not contain magnetite and corresponds to maghemite. As a result of their low concentration, signals for Cu nanoparticles (NPs) were not observed in the XRD pattern of $\gamma\text{-Fe}_2\text{O}_3\text{-Cu}$ (Figure 1).

The nature of the Cu on the surface of maghemite was confirmed by XPS. The spectrum shows the presence of Cu^0 and CuO from the doublet peaks at a binding energy (BE) of 932.49 and 952.29 eV (assigned to $\text{Cu}2p_1$) and BE = 933.67 and 953.46 eV (assigned to $\text{Cu}2p_3$), which match perfectly with the positions of Cu^0 and CuO , respectively (Figure 2).^[30]

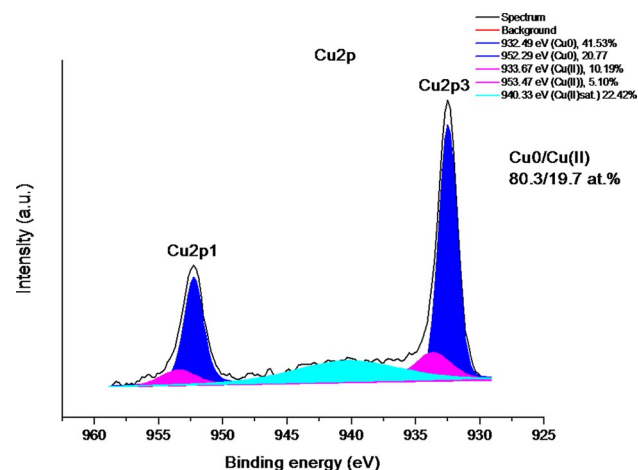


Figure 2. XPS spectrum of the maghemite-Cu nanocatalyst (Cu 2p spectrum).

To exclude the presence of the Cu^+ valence state, the Auger Cu LMM spectrum was acquired (Figure S2), and no evidence of Cu^+ ions was found.

The Cu content in catalyst was found to be 4.7 mol% by AAS (Figure S1). TEM analysis of the maghemite-Cu material revealed that the overall diameter of the as-synthesized NPs was in the range 20–40 nm (Figure 3). EDS and HAADF-STEM images of the maghemite-Cu nanocatalyst are shown in (Fig-

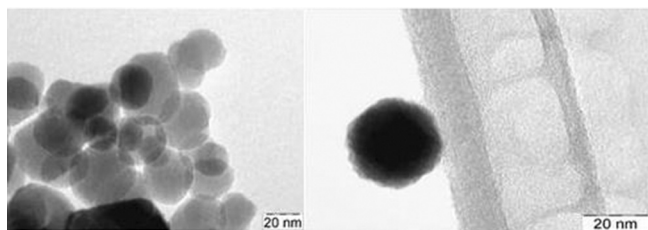


Figure 3. TEM images of the maghemite-Cu nanocatalyst.

ure 4a–f). The EDS profile indicates the presence of Fe and Cu species in the catalysts clearly (Figure 4f). Element mapping of maghemite-Cu revealed that the Cu NPs are dispersed uniformly on the surface of maghemite. The element mapping of C is not revealed because a huge amount of C exists in the support film of the TEM grid. Cu NPs are distributed on the surface of maghemite (Scheme 2), which is confirmed by HAADF-STEM images (Figure 4b). The phase identification, chemical nature, and magnetic properties were analyzed by Mössbauer spectroscopy. The ^{57}Fe Mössbauer spectra of the studied material were measured (Figure 5) by employing a MS2007 Mössbauer spectrometer^[31,32] that was operated at a constant acceleration mode and equipped with a ^{57}Co (Rh) source. At room temperature, the Mössbauer spectrum of the sample shows one slightly asymmetrical sextet component (Figure 5), for which the values of the hyperfine parameters (Table S1) approach those reported for a gamma-phase ($\gamma\text{-Fe}_2\text{O}_3$) iron(III) oxide.^[33,34] The distribution of the hyperfine magnetic field (B_{hf}) was applied to fit the spectrum correctly because of the non-Lorentzian profile of the Mössbauer resonant lines. This feature is typical for $\gamma\text{-Fe}_2\text{O}_3$ nanoparticles and implies an evolution of the collective magnetic excitations as the nanoparticle superspin rotates around the particularly easy axis of magnetization established by the magnetic anisotropy of the particle.^[35]

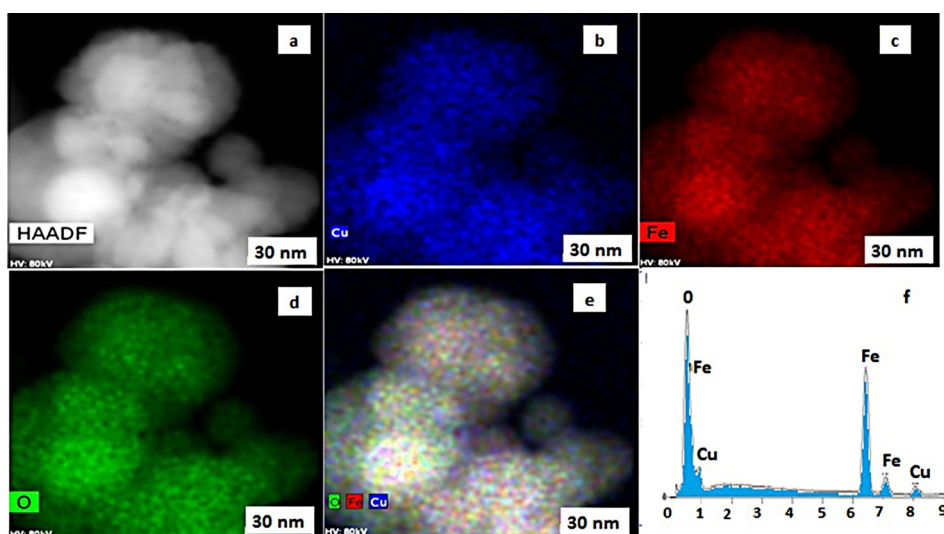


Figure 4. HAADF-STEM images of the maghemite-Cu nanocatalyst; a) HAADF image that shows Cu at 30 nm; b) HAADF image that shows Cu; c) HAADF image that shows Fe; d) HAADF image that shows O; e) HAADF image that shows Cu, Fe, and O together in maghemite-Cu at 30 nm; f) EDS spectrum that indicates the presence of Cu.

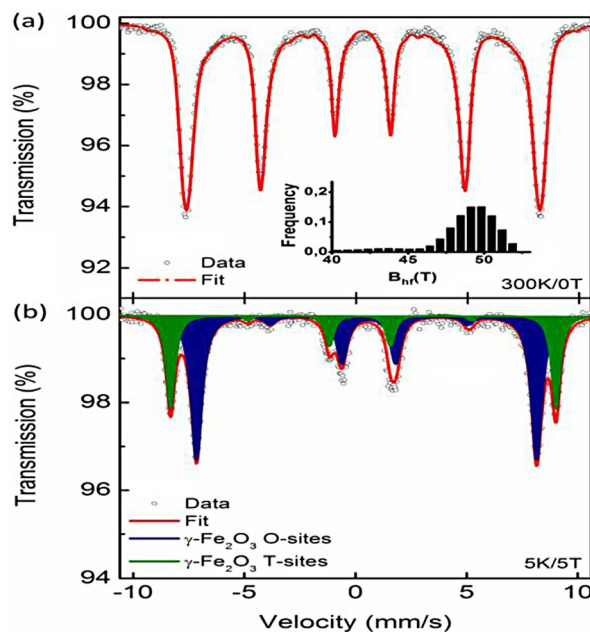


Figure 5. ^{57}Fe Mössbauer spectra of the maghemite-Cu nanocatalyst recorded a) at room temperature without an external magnetic field, b) at 5 K with a magnetic field of 5 T. Inset in a shows the distribution of the hyperfine magnetic field used to evaluate the room-temperature spectrum.

Furthermore, $\gamma\text{-Fe}_2\text{O}_3$ NPs are in a magnetically blocked state because no doublet (superparamagnetic) component is observed in the spectrum and they have an average blocking temperature higher than 300 K with respect to the timeframe of the Mössbauer technique ($\sim 10^{-8}$ s), which indicates that the NPs in the system are bigger than 15 nm.^[34] At a lower temperature (5 K) and with the application of an external magnetic field (low-temperature irradiation facility, LTIF; 5 T), the Mössbauer spectrum of the sample is split into two sextets (Figure 5). The first sextet that has a lower isomer shift (δ) and higher hyperfine magnetic field (B_{eff}) represents Fe ions in the

T sites of the $\gamma\text{-Fe}_2\text{O}_3$ spinel crystal structure and the other sextet that has a higher δ and lower B_{eff} represents $\gamma\text{-Fe}_2\text{O}_3$ O sites. The hyperfine parameters of the sextets are given in Table S1. The isomer shifts of both sextets fall in the range reported for a high-spin ($S=5/2$) Fe^{3+} state, and no other spectral components are observed. The synthesized maghemite-Cu nanocatalyst has a single-phase character without any admixtures of iron oxide, and the spectral ratio of T/O is close to 1:1.94, which reflects the non-stoichiometric nature of maghemite, probably because of the occurrence of vacancies at the T sites.^[34] Under these conditions

(5 K, 5 T) the two sextets are better resolved by comparing the low-temperature spectrum with that without an external magnetic field as B_{ext} adds to the B_{hf} value of the T and O sextets.^[34]

Moreover, the second and fifth lines of both subspectra are almost suppressed, which indicates that the atomic magnetic moments that belong to the T and O sites almost perfectly align to and against the direction of B_{ext} , respectively. This implies that the spin-canting phenomenon is not evolved.^[34] The analysis also revealed that the NPs in the assembly are larger than ~10 nm as the second and fifth lines in the LTIF Mössbauer spectrum (of both subspectra) are almost suppressed. Here, the spin-canting phenomenon appears only slightly for smaller particles in the assembly because of the particle size distribution, which is in accordance with the utilized the hyperfine field distribution. The nonzero values of the quadrupole splitting parameter (ΔE_Q) reflect the interaction of maghemite nanoparticles with Cu on their surface; the adsorption of Cu probably alters the surrounding or the surface NP atoms, which causes the electronic charge to deviate from spherical symmetry.^[36]

Herein, the catalytic efficiency of the maghemite-Cu nanocatalyst was investigated using 4-hydroxytoluene (**1a**) and iodobenzene (**2a**) as model substrates (Table 1). The effect of vari-

Table 1. Optimization of reaction.^[a]



Entry	Base	Solvent [mL]	Catalyst [mg]	T [°C]	t [h]	Yield [%]
1	Na ₂ CO ₃	DMF	80	130	24	31
2	K ₂ CO ₃	DMF	80	130	24	58
3	Cs ₂ CO ₃	DMF	80	130	24	94
4	Cs ₂ CO ₃	Toluene	80	130	24	63
5	Cs ₂ CO ₃	DMSO	80	130	24	84
6	Cs ₂ CO ₃	DMF	no catalyst	130	48	trace
7	Cs ₂ CO ₃	DMF	40	130	24	80
8	Cs ₂ CO ₃	DMF	50	130	24	94
9	Cs ₂ CO ₃	DMF	50	90	24	67
10	Cs ₂ CO ₃	DMF	50	150	24	94

[a] Reaction conditions: 4-hydroxytoluene (1 mmol), iodobenzene (1 mmol), base (2 equiv.), solvent (3 mL), maghemite-Cu (40–80 mg; 2.9–5.9 mol%), 130 °C, 24 h, N₂ atmosphere.

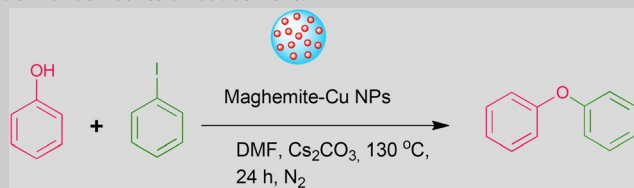
ous important parameters such as the amount of catalyst, temperature, solvent, and base were investigated to obtain an optimum reaction profile for the cross-coupling reaction. Notably, cesium carbonate was the best base with maghemite-Cu compared to potassium carbonate and sodium carbonate in DMF at 130 °C under N₂ and gave the desired product selectively in 94% yield (Table 1, entries 1–3 and 8). The coupling reaction also worked well in other organic solvents, which included DMSO and toluene, but DMF appeared to be the best (Table 1, entries 3–5). Control experiments confirmed that no conversion occurred without catalyst even after 48 h of reaction (Table 1, entry 6). The highest yield was attained if the catalyst loading

was elevated to 50 mg. However, there was no increase in the yield if catalyst was added beyond this amount (Table 1, entries 3, 7, and 8). The effect of temperature was also investigated. At a high temperature of 130 °C, an excellent yield was obtained, but no further enhancement in conversion was observed at 150 °C (Table 1, entries 8–10).

After the optimization of the reaction parameters, the catalytic activity of the maghemite-Cu nanocatalyst was examined for the C–O (O-arylation) cross-coupling reaction with various derivatives of phenols and substituted aryl iodides (Table 2). Notably, the presence of an electron-donating group, such as Me, OMe, and tBu, on the phenol groups at the *para* positions provided good to excellent yields (Table 2, entries 2–8); whereas comparatively lower yields were obtained because of the steric effect at the *ortho/meta* position of phenols (Table 2, entries 9–11). Interestingly, naphthalene homologues of phenol, such as 2-naphthol, gave excellent yields of the corresponding products (Table 2, entry 12). The versatility of the maghemite-Cu nanocatalyst was also explored for the S- and N-arylation of substituted thiophenol, aniline, imidazole, thiophenols, indole, and pyrazole with aryl iodide (Table 3). We observed that phenyl iodide with an electron-withdrawing group (NO₂) at the *para* position gave excellent yields (Table 3, entries 1–6), whereas an electron-donating group (Me) at the *para* position gave low to moderate yields (Table 3, entries 7–9). Furthermore, the N-arylation of aniline, indole, pyrrole, and imidazole with iodobenzene gave good yields of the corresponding coupled products (Table 3, entries 10–14).

The recovery and reusability of a catalyst are the two important factors that need to be evaluated, thus the recyclability of the maghemite-Cu nanocatalyst was examined in the reaction of 4-hydroxyphenol and phenyl iodide under identical optimized experimental conditions. In each cycle, the catalyst was separated magnetically, washed with ethanol, and dried at 60 °C under vacuum to remove residual solvents. The yields were 94, 93, 93, 92, 90, and 88% from the first to the sixth cycle, respectively. The FTIR spectra of the fresh and recycled catalysts (after the sixth run) were very similar (Figure S3). This means that the efficiency of the catalyst is unaltered during the reaction, hence the maghemite-Cu nanocatalyst is a benign catalyst in terms of recovery and recyclability. We also performed a leaching study of Cu metal by AAS, and the results revealed that the concentration of Cu in the filtrate was negligible (<0.1 ppm). Additionally, UV/Vis spectroscopic studies showed no absorption peak of Cu metal in the supernatant of the reaction mixture (data not shown). The reason behind the decrease in yield could be explained in terms of the agglomeration and aggregation of the Cu nanocatalyst into large particles. This result showed that there was barely any change in the amount of Cu compared with that of the fresh catalyst. A proposed mechanism is illustrated in Figure 6. The reaction is assumed to occur through oxidative addition followed by reductive elimination. Initially, the nucleophile adds to the maghemite-Cu nanocatalyst to form complex I, which reacts oxidatively with Ar–X to form complex II, and this intermediate finally bestows the desired product III by reductive elimination in the presence of base.^[37]

Table 2. Maghemite-Cu catalyzed C–O cross-coupling (O-arylation) of substituted phenols with derivatives of iodobenzene.^[a]



Entry	Aryl iodide	Phenol	Product	Yield ^[b] [%]
1				87
2				94
3				99
4				98
5				99
6				99
7				98
8				99
9				88
10				36
11				13
12				93

[a] Reaction conditions: phenol (1 mmol), aryl iodide (1 mmol), Cs₂CO₃ (2 equiv.), DMF (3 mL), maghemite-Cu (50 mg), 130 °C, 24 h, N₂ atmosphere. [b] GC–MS yield.

Conclusions

We have prepared a viable, versatile, ligand-free, and magnetically separable heterogeneous maghemite-Cu nanocatalyst for different types of C–O, C–N, and C–S cross-coupling reactions. This catalyst was prepared from inexpensive precursors using

a simple impregnation procedure without the use of cumbersome linkers or ligands. Furthermore, the cross-coupling reactions proceeded successfully and were convincingly superior in terms of yield. This may be attributed to the nanometer size of the maghemite solid support material, which allowed the immobilization of a high amount of complex and enhanced the dispersion of the catalytically active sites in the reaction medium and thus improved their accessibility to the substrate. In addition, a hot filtration test was performed, which suggested that the nanocatalyst catalyzes the cross-coupling reaction in a truly heterogeneous manner. Thus, the salient features of the catalyst lie in its simplicity, economic feasibility, liberty from complex ligands, and excellent yields without the need for traditional filtration, which makes it an attractive and sustainable option.

Experimental Section

Powder XRD patterns of iron oxide samples were recorded at RT by using an X'Pert PRO MPD diffractometer (PANalytical) in Bragg–Brentano geometry with iron-filtered CoK_α radiation (40 kV, 30 mA, λ = 0.1789 nm) and equipped with an X'Celerator detector, programmable divergence, and diffracted beam antiscatter-slits. The angular range of measurement was set as 2θ = 10–105° with a step size of 0.017°. The crystalline phases in the experimental XRD patterns were identified by using the X'Pert High Score Plus software that includes a PDF-4+ and ICSD databases. (Sample preparation: grinding if needed and compression in the sample holder with a flat glass. The sample area in the sample holder is ≈ 2 cm²). TEM images were obtained by using a Hitachi H8100 microscope with a ThermoNoran light elements EDS detector and a charge-coupled device (CCD) camera for image acquisition. The maghemite-Cu fine powder was placed on a carbon stub, and the images were recorded at 5–15 kV by using a large-field detector (LFD) under low vacuum. Elemental analysis was performed by using a light elements EDS detector from Oxford. The maghemite-Cu powder was spread on a double-sided carbon tape and analyzed using an acceleration voltage of 25 kV. Microscopic images were obtained by using a HRTEM TITAN 60–300 with X-FEG-type emission gun that was operated at 80 kV. The point resolution is better than 0.08 nm in TEM mode. Elemental mapping was obtained by STEM-EDS with an acquisition time of 20 min. Sample preparation: The powder samples were dispersed in ethanol and ultrasonicated for 5 min. One drop of this solution was placed on a copper grid with a holey carbon film. The sample was dried at RT. For surface investigation, a PHI 5000 VersaProbe II XPS system (Physical Electronics) with monochromatic AlK_α source (15 kV, 50 W) and photon energy of 1486.7 eV was employed. Dual-beam charge compensation was used for all measurements. All the spectra were measured under a vacuum of 1.6 × 10^{−7} Pa at RT (22 °C). The survey spectra was measured with a pass energy of 187.850 eV and an electronvolt step of 0.8 eV, whereas a pass energy of 23.500 eV and electronvolt step of 0.2 eV were

Table 3. Maghemite-Cu catalyzed C–S and C–N cross-coupling (N- and S-arylation) of thiophenol, aniline, indole, imidazole, and pyrrole with substituted iodobenzenes.^[a]

Entry	Aryl halide	Phenyl–Nu–H	Product	Yield ^[b] [%]
1				98
2				99
3				98
4				98
5				97
6				99
7				50
8				67
9				77
10				99
11				98
12				99
13				82
14				99

[a] Reaction conditions: nucleophile (1 mmol), aryl iodide (1 mmol), Cs₂CO₃ (2 equiv.), DMF (3 mL), maghemite-Cu (50 mg), 130 °C, 24 h, N₂ atmosphere. [b] GC–MS yield.

used for the high-resolution spectra. Dual-beam charge compensation was set up for all measurements. The spectra were evaluated by using the MultiPak (Ulvac-Phi, Inc.) software. All BE values were referenced to the C 1s carbon peak at BE = 284.80 eV.

Catalyst preparation

Preparation of maghemite (γ -Fe₂O₃)

Typically, FeSO₄·7H₂O (6.06 g, 21.79 mmol) and FeCl₃·6H₂O (11.75 g, 45.08 mmol) were dissolved in de-ionized water (100 mL, previously degassed with N₂) under a N₂ atmosphere. The resulting mixture was stirred for 15 min and heated at 60 °C under vigorous stirring. When the temperature reached 60 °C, aqueous NH₂OH (25 mL, 25–28% w/w) was added dropwise, a black precipitate formed immediately, and heating was continued for 2 h under a N₂ atmosphere. After vigorous stirring for 2 h, the precipitate was separated magnetically and washed thoroughly with water until the supernatant liquor reached neutrality. The obtained material was dried in an oven at 100 °C for 12 h, and 75% yield of maghemite was obtained.

Preparation of maghemite-Cu nanocatalyst

Maghemite (2 g) and CuCl₂ (for 5 wt% of Cu on maghemite) were stirred at RT in aqueous solution (50 mL) for 1 h. After impregnation, the suspension was adjusted to pH 12–13 by adding sodium hydroxide (1.0 M) and further stirred for 20 h. The solid was collected and washed with distilled water (5 × 20 mL). The resulting maghemite-Cu NPs were sonicated for 10 min, washed with distilled water and subsequently with ethanol, and dried under vacuum at 60 °C for 24 h. The Cu content was found to be 4.7% using AAS.

Experimental procedure for the cross-coupling (C–O, C–N, C–S) reactions catalyzed by the maghemite-Cu nanocatalyst

In an oven-dried 10 mL round-bottomed flask, aryl iodide (1 mmol), phenol/imidazole/aniline/thiophenol/pyrrole (1 mmol), and Cs₂CO₃ (2 equiv.) were stirred in DMF (3 mL), and the catalyst (50 mg) was added under N₂. The resulting mixture was stirred at 130 °C in an oil bath for 24 h. The progress of reaction was monitored by TLC and GC–MS. After the completion of the reaction, the catalyst was recovered with an external magnet and then washed with ethanol and water. The obtained catalyst was dried under vacuum at 60 °C and reused in the next run. The reaction mixture was diluted with water and extracted by ethyl acetate (3 × 30 mL). The combined organic layers were dried over anhydrous Na₂SO₄ and analyzed by GC–MS.

Acknowledgements

R.G. expresses her gratitude to the University Grand Commission, Delhi, India for the award of junior re-

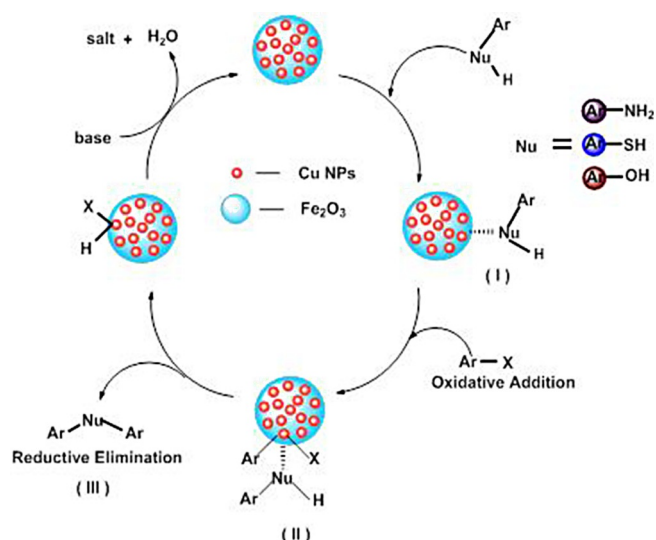


Figure 6. Proposed reaction mechanism.

search fellowship. Also, thanks are given to USIC-CLF, University of Delhi. The authors acknowledge support from the Ministry of Education, Youth and Sports of the Czech Republic (LO1305) and by the Operational Program Education for Competitiveness - European Social Fund (project CZ.1.07/2.3.00/30.0041 and CZ.1.07/2.4.00/31.0189) of the Ministry of Education, Youth and Sports of the Czech Republic. M.P. gratefully acknowledges the financial support from the internal student grant IGA of Palacký University in Olomouc, Czech Republic, (IGA-PrF-2015-017).

Keywords: copper · cross-coupling · heterogeneous catalysis · magnetism · sustainable chemistry

- [1] a) R. S. Varma, *Green Chem.* **2014**, *16*, 2027–2041; b) Z. Guo, B. Liu, Q. Zhang, W. Deng, Y. Wang, Y. Yang, *Chem. Soc. Rev.* **2014**, *43*, 3480–3524; c) R. Hudson, Y. Feng, R. S. Varma, A. Moores, *Green Chem.* **2014**, *16*, 4493–4505.
- [2] a) M. B. Gawande, R. Luque, R. Zboril, *ChemCatChem* **2014**, *6*, 3312–3313; b) D. Wang, D. Astruc, *Chem. Rev.* **2014**, *114*, 6949–6985; c) R. K. Sharma, Y. Monga, A. Puri, G. Gaba, *Green Chem.* **2013**, *15*, 2800–2809; d) K. V. Ranganath, J. Kloesges, A. H. Schäfer, F. Glorius, *Angew. Chem. Int. Ed.* **2010**, *49*, 7786–7789; *Angew. Chem.* **2010**, *122*, 7952–7956.
- [3] a) I. I. Slowing, B. G. Trewyn, S. Giri, V. S. Y. Lin, *Adv. Funct. Mater.* **2007**, *17*, 1225–1236; b) I. I. Slowing, J. L. Vivero-Escoto, B. G. Trewyn, V. S. Y. Lin, *J. Mater. Chem.* **2010**, *20*, 7924–7937; c) M. Pagliaro, R. Ciriminna, G. Palmisano, *J. Mater. Chem.* **2009**, *19*, 3116–3126; d) J. M. Rosenholm, C. Sahlgren, M. Linden, *Nanoscale* **2010**, *2*, 1870–1883.
- [4] a) S. Chaturvedi, P. N. Dave, N. K. Shah, *J. Saudi Chem. Soc.* **2012**, *16*, 307–325; b) K. H. Park, K. Jang, S. U. Son, D. A. Sweigart, *J. Am. Chem. Soc.* **2006**, *128*, 8740–8741.
- [5] a) R. K. Sharma, A. Pandey, S. Gulati, A. Adholeya, *Chem. Eng. J.* **2012**, *210*, 490–499; b) R. K. Sharma, A. Pandey, S. Gulati, A. Adholeya, *J. Hazard. Mater.* **2012**, *209*, 285–292; c) R. K. Sharma, Y. Monga, *Appl. Catal. A* **2013**, *454*, 1–10.
- [6] a) J. E. Mondloch, Q. Wang, A. I. Frenkel, R. G. Finke, *J. Am. Chem. Soc.* **2010**, *132*, 9701–9714; b) S. Miao, C. Zhang, Z. Liu, B. Han, Y. Xie, S. Ding, Z. Yang, *J. Phys. Chem. C* **2008**, *112*, 774–780; c) S. Ko, J. Jang, *Angew. Chem. Int. Ed.* **2006**, *45*, 7564–7567; *Angew. Chem.* **2006**, *118*, 7726–7729; d) S. C. Tsang, V. Caps, I. Paraskevas, D. Chadwick, D. Thompsett, *Angew. Chem. Int. Ed.* **2004**, *43*, 5645–5649; *Angew. Chem.* **2004**, *116*, 5763–5767; e) M. Zhu, G. Diao, *Nanoscale* **2011**, *3*, 2748–2767; f) B. Liu, W. Zhang, F. Yang, H. Feng, X. Yang, *J. Phys. Chem. C* **2011**, *115*, 15875–15884.
- [7] a) S. Shylesh, V. Schünemann, W. R. Thiel, *Angew. Chem. Int. Ed.* **2010**, *49*, 3428–3459; *Angew. Chem.* **2010**, *122*, 3504–3537; b) V. Polshettiwar, R. Luque, A. Fihri, H. Zhu, M. Bouhrara, J. M. Basset, *Chem. Rev.* **2011**, *111*, 3036–3075; c) R. N. Baig, R. S. Varma, *Chem. Commun.* **2013**, *49*, 752–770; d) D. Zhang, C. Zhou, Z. Sun, L.-Z. Wu, C.-H. Tung, T. Zhang, *Nanoscale* **2012**, *4*, 6244–6255; e) H. Song, *Acc. Chem. Res.* **2015**, *48*, 491–499.
- [8] S. R. Kale, S. S. Kahandal, M. B. Gawande, R. V. Jayaram, *RSC Adv.* **2013**, *3*, 8184–8192.
- [9] M. B. Gawande, P. S. Branco, R. S. Varma, *Chem. Soc. Rev.* **2013**, *42*, 3371–3393.
- [10] R. B. N. Baig, R. S. Varma, *Chem. Commun.* **2012**, *48*, 2582–2584.
- [11] B. R. Vaddula, A. Saha, J. Leazer, R. S. Varma, *Green Chem.* **2012**, *14*, 2133–2136.
- [12] A. Rezaeifard, M. Jafarpour, P. Farshid, A. Naeimi, *Eur. J. Inorg. Chem.* **2012**, 5515–5524.
- [13] P.-H. Li, B.-L. Li, Z.-M. An, L.-P. Mo, Z.-S. Cui, Z.-H. Zhang, *Adv. Synth. Catal.* **2013**, *355*, 2952–2959.
- [14] a) B. C. Ranu, R. Dey, T. Chatterjee, S. Ahammed, *ChemSusChem* **2012**, *5*, 22–44; b) S. V. Ley, A. W. Thomas, *Angew. Chem. Int. Ed.* **2003**, *42*, 5400–5449; *Angew. Chem.* **2003**, *115*, 5558–5607; c) P. F. Larsson, A. Correa, M. Carril, P. O. Norrby, C. Bolm, *Angew. Chem. Int. Ed.* **2009**, *48*, 5691–5693; *Angew. Chem.* **2009**, *121*, 5801–5803.
- [15] a) G. Evano, N. Blanchard, M. Toumi, *Chem. Rev.* **2008**, *108*, 3054–3131; b) G. Evano, C. Theunissen, A. Pradal, *Nat. Prod. Rep.* **2013**, *30*, 1467–1489; c) F. Hervás, G. Morreale de Escobar, F. Escobar del Rey, *Endocrinology* **1976**, *98*, 77–83; d) M. Kožisek, J. Bray, P. Řezáčová, K. Šašková, J. Brynda, J. Pokorná, J. Konvalinka, *J. Mol. Biol.* **2007**, *374*, 1005–1016.
- [16] a) J. Hassan, M. Sevignon, C. Gozzi, E. Schulz, M. Lemaire, *Chem. Rev.* **2002**, *102*, 1359–1470; b) S. V. Ley, A. W. Thomas, *Angew. Chem. Int. Ed.* **2003**, *42*, 5400–5449; *Angew. Chem.* **2003**, *115*, 5558–5607; c) M. E. Jung, D. Jachiet, J. C. Rohtoff, *Tetrahedron Lett.* **1989**, *30*, 4211–4214; d) R. K. Gujadhur, C. G. Bates, D. Venkataraman, *Org. Lett.* **2001**, *3*, 4315–4317; e) C. Palomo, M. Oiarbide, R. Lopez, E. Gomez-Bengoia, *Chem. Commun.* **1998**, 2091–2092.
- [17] a) R. A. Widenhoefer, H. A. Zhong, S. L. J. Buchwald, *J. Am. Chem. Soc.* **1997**, *119*, 6787–6795; b) J. P. Wolfe, J. F. Marcoux, S. L. Buchwald, *Acc. Chem. Res.* **1998**, *31*, 805–818; c) D. Zim, S. L. Buchwald, *Org. Lett.* **2003**, *5*, 2413–2415; d) M. C. Harris, X. Huang, S. L. Buchwald, *Org. Lett.* **2002**, *4*, 2885–2888; e) J. P. Wolfe, H. Tomori, J. P. Sadighi, J. Yin, S. L. Buchwald, *Org. Chem.* **2000**, *65*, 1158–1174; f) S. I. Kuwabe, K. E. Torraca, S. L. Buchwald, *J. Am. Chem. Soc.* **2001**, *123*, 12202–12206.
- [18] a) J. F. Hartwig, *Acc. Chem. Res.* **1998**, *31*, 852; b) J. F. Hartwig, *Angew. Chem. Int. Ed.* **1998**, *37*, 2046–2067; *Angew. Chem.* **1998**, *110*, 2154–2177; c) G. Mann, C. Incarvito, A. L. Rheingold, J. F. Hartwig, *J. Am. Chem. Soc.* **1999**, *121*, 3224–3225.
- [19] a) D. A. Evans, J. L. Katz, T. R. West, *Tetrahedron Lett.* **1998**, *39*, 2937–2940; b) C. Decicco, P. S. Song, D. A. Evans, *Org. Lett.* **2001**, *3*, 1029–1032.
- [20] D. M. T. Chan, K. L. Monaco, R. Wang, M. P. Winters, *Tetrahedron Lett.* **1998**, *39*, 2933–2936.
- [21] a) A. Aranyos, D. W. Old, A. Kiyomori, J. P. Wolfe, J. P. Sadighi, S. L. Buchwald, *J. Am. Chem. Soc.* **1999**, *121*, 4369–4378; b) D. Ma, Q. Cai, H. Zhang, *Org. Lett.* **2003**, *5*, 2453–2455.
- [22] a) G. A. Molander, L. Jean-Gérard, *J. Org. Chem.* **2009**, *74*, 1297–1303; b) G. A. Molander, T. Ito, *Org. Lett.* **2001**, *3*, 393–396; c) S. Sueki, Y. Kuni-nobu, *Org. Lett.* **2013**, *15*, 1544–1547.
- [23] a) H. Z. Yu, Y. Y. Jiang, Y. Fu, L. Liu, *J. Am. Chem. Soc.* **2010**, *132*, 18078–18091; b) D. Ma, Q. Cai, *Org. Lett.* **2003**, *5*, 3799–3802; c) C. T. Yang, Y. Fu, Y. B. Huang, J. Yi, Q. X. Guo, L. Liu, *Angew. Chem. Int. Ed.* **2009**, *48*, 7398–7401; *Angew. Chem.* **2009**, *121*, 7534–7537; d) F. Y. Kwong, S. L. Buchwald, *Org. Lett.* **2003**, *5*, 793–796; e) F. Y. Kwong, A. Klapars, S. L. Buchwald, *Org. Lett.* **2002**, *4*, 581–584.
- [24] a) M. Hosseini-Sarvari, Z. Razmi, *RSC Adv.* **2014**, *4*, 44105–44116; b) H. Joshi, K. N. Sharma, A. K. Sharma, A. K. Singh, *Nanoscale* **2014**, *6*, 4588–4597; c) Z. Jiang, J. She, X. Lin, *Adv. Synth. Catal.* **2009**, *351*, 2558–2562.
- [25] a) P. Zhang, J. Yuan, H. Li, X. Liu, X. Xu, M. Antonietti, Y. Wang, *RSC Adv.* **2013**, *3*, 1890–1895; b) K. Swapna, S. N. Murthy, M. T. Jyothi, Y. V. D. Nageswar, *Org. Biomol. Chem.* **2011**, *9*, 5978–5988; c) N. Salam, S. K.

- Kundu, A. S. Roy, P. Mondal, S. Roy, A. Bhaumik, S. M. Islam, *Catal. Sci. Technol.* **2013**, *3*, 3303–3316; d) J. Mondal, A. Modak, A. Dutta, A. Bhaumik, *Dalton Trans.* **2011**, *40*, 5228–5235; e) H. J. Xu, Y. F. Liang, X. F. Zhou, Y. S. Feng, *Org. Biomol. Chem.* **2012**, *10*, 2562–2568; f) D. Saberi, M. Sheykhan, K. Niknam, A. Heydari, *Catal. Sci. Technol.* **2013**, *3*, 2025–2031; g) M. Wang, B. Yuan, T. Ma, H. Jiang, Y. Li, *RSC Adv.* **2012**, *2*, 5528–5530; h) S. L. Buchwald, C. Bolm, *Angew. Chem. Int. Ed.* **2009**, *48*, 5586–5587; *Angew. Chem.* **2009**, *121*, 5694–5695.
- [26] a) B. H. Lipshutz, D. M. Nihan, E. Vinogradova, B. R. Taft, Z. V. Boskovic, *Org. Lett.* **2008**, *10*, 4279–4282; b) A. K. Gupta, G. Tirumaleswara Rao, K. N. Singh, *Tetrahedron Lett.* **2012**, *53*, 2218–2221.
- [27] a) M. B. Gawande, S. N. Shelke, R. Zboril, R. S. Varma, *Acc. Chem. Res.* **2014**, *47*, 1338–1348; b) M. B. Gawande, A. K. Rath, I. D. Nogueira, R. S. Varma, P. S. Branco, *Green Chem.* **2013**, *15*, 1895–1899; c) A. Panáček, R. Prucek, J. Hrbac, T. Nevecna, J. Steffkova, R. Zboril, L. Kvitek, *Chem. Mater.* **2014**, *26*, 1332–1339.
- [28] M. B. Gawande, A. K. Rath, P. S. Branco, I. D. Nogueira, A. Velhinho, J. J. Shrikhande, U. U. Indulkar, R. V. Jayaram, C. A. A. Ghumman, N. Bundaleski, O. M. N. D. Teodoro, *Chem. Eur. J.* **2012**, *18*, 12628–12632.
- [29] M. B. Gawande, V. D. B. Bonifacio, R. S. Varma, I. D. Nogueira, N. Bundaleski, C. A. A. Ghumman, O. M. N. D. Teodoro, P. S. Branco, *Green Chem.* **2013**, *15*, 1226–1231.
- [30] a) M. C. Biesinger, L. W. M. Lau, A. R. Gerson, R. S. C. Smart, *Appl. Surf. Sci.* **2010**, *257*, 887–898; b) S. N. Shelke, S. R. Bankar, G. R. Mhaske, S. S. Kadam, D. K. Murade, S. B. Bhorkade, M. B. Gawande, *ACS Sustainable Chem. Eng.* **2014**, *2*, 1699–1706.
- [31] J. Pechoušek, D. Jančík, J. Frydrych, J. Navařík, P. Novák, *AIP Conf. Proc.* **2012**, *1489*, 186–193.
- [32] J. Pechoušek, R. Prochazka, D. Jančík, J. Frydrych, M. Mashlan, *J. Phys. Conf. Ser.* **2010**, *217*, 012006.
- [33] J. Tuček, P. Tuček, J. Čuda, J. Filip, J. Pechoušek, L. Machala, R. Zbořil, *AIP Conf. Proc.* **2012**, *1489*, 56–74.
- [34] J. Tuček, R. Zboril, D. Petridis, *J. Nanosci. Nanotechnol.* **2006**, *6*, 926–947.
- [35] J. Tuček, L. Machala, J. Frydrych, J. Pechoušek, R. Zbořil in *Mössbauer Spectroscopy: Applications in Chemistry, Biology, and Nanotechnology* (Eds.: V. K. Sharma, G. Klingelhofer, T. Nishida), Wiley, **2013**, pp. 351–392.
- [36] N. N. Greenwood, T. C. Gibb, *Mössbauer Spectroscopy*, Chapman&Hall Ltd., London, **1971**.
- [37] a) L. Rout, S. Jammi, T. Punniyamurthy, *Org. Lett.* **2007**, *9*, 3397–3399; b) B. Sreedhar, R. Arundhathi, P. L. Reddy, M. L. Kantam, *J. Org. Chem.* **2009**, *74*, 7951–7954.

Received: May 16, 2015

Revised: July 13, 2015

Published online on September 17, 2015